FOCUS ISSUE OF SELECTED PAPERS FROM IMLB 2016 WITH INVITED PAPERS CELEBRATING 25 YEARS OF LITHIUM ION BATTERIES

A Guide to Ethylene Carbonate-Free Electrolyte Making for Li-Ion Cells

Lin Ma,[a,*] S. L. Glazier,[b] R. Petibon,[a] Jian Xia,[b,*] Jeremy M. Peters,[b] Q. Liu,[b,c] J. Allen,[b] R. N. C. Doig,[d] and J. R. Dahn[a,b,,z]**

[a]*Department of Chemistry, Dalhousie University, Halifax B3H 4R2, Canada*
[b]*Department of Physics and Atmospheric Science, Dalhousie University, Halifax B3H 3J5, Canada*
[c]*MIIT Key Laboratory of Critical Materials Technology for New Energy Conversion and Storage, School of Chemistry and Chemical Engineering, Harbin Institute of Technology, Harbin 150001, People's Republic of China*
[d]*Department of Mathematics and Statistics, Dalhousie University, Halifax B3H 4R2, Canada*

$Li[Ni_{0.42}Mn_{0.42}Co_{0.16}]O_2$ (NMC442)/graphite pouch cells demonstrate superb performance at high voltage when ethylene carbonate (EC)-free electrolytes, using a solvent mixture that is >95% ethyl methyl carbonate (EMC) and between 2 and 5% of an "enabler", are used. The "enablers", required to passivate graphite during formation, can be vinylene carbonate (VC), methylene-ethylene carbonate (MEC), fluoroethylene carbonate (FEC) or difluoro ethylene carbonate (DiFEC), among others. In order to optimize the amount of "enabler" added to EMC, gas chromatography coupled with mass spectrometry (GC-MS) was used to track the consumption of "enabler" during the formation step. Storage tests, electrochemical impedance spectroscopy (EIS), ultrahigh precision coulometry (UHPC), long-term cycling, differential voltage analysis and isothermal microcalorimetry were used to determine the optimum amount of enabler to add to the cells. It was found that the graphite negative electrode cannot be fully passivated when the amount of "enabler" is too low resulting in gas production and capacity fade. Using excess "enabler" can cause large impedance and gas production in most cases. The choice of "enabler" also impacts cell performance. A solvent blend of 5% FEC with 95% EMC (by weight) provides the best combination of properties in NMC442/graphite cells operated to 4.4 V. It is our opinion that the experiments and their interpretation presented here represent a primer for the design of EC-free electrolytes.

© The Author(s) 2016. Published by ECS. This is an open access article distributed under the terms of the Creative Commons Attribution 4.0 License (CC BY, http://creativecommons.org/licenses/by/4.0/), which permits unrestricted reuse of the work in any medium, provided the original work is properly cited. [DOI: 10.1149/2.0191701jes] All rights reserved.

Manuscript submitted September 30, 2016; revised manuscript received November 2, 2016. Published November 17, 2016. *This paper is part of the Focus Issue of Selected Papers from IMLB 2016 with Invited Papers Celebrating 25 Years of Lithium Ion Batteries.*

Lithium-ion batteries (LIB) are now widely used in electrified vehicles and energy storage systems.[1] These applications require longer calendar and cycle lifetime as well as higher energy density. In order to increase the energy density of LIB, researchers focus on developing electrode materials with high specific capacity that may involve charging to increased upper cutoff potentials.[2,3]

Several methods have been investigated to allow LIB to use higher cutoff potentials without compromising their lifetime. Sun et al.[4] and Hu et al.[5] showed that AlF_3 or ZrO_2-coatings improved the rate capability, cycling stability and interface stability for $Li[Ni_{1/3}Mn_{1/3}Co_{1/3}]O_2$ (NMC111)/Li half cells operated to 4.5 V. Nie et al.[6,7] used electrolyte additives in traditional ethylene carbonate (EC)-based electrolyte, to create $Li[Ni_{0.42}Mn_{0.42}Co_{0.16}]O_2$ (NMC442)/graphite pouch cells that demonstrated excellent capacity retention, low impedance growth and high coulombic efficiency (CE) at up to 4.5 V.

Alternative solvents are another way of extending the potential operating range for LIB. Fluorinated solvents,[8,9] dinitriles[10] or sulfones[11,12] are of interest because their oxidation potentials are higher than that of traditional alkyl carbonate solvents.[13] However these alternative solvents have disadvantages such as high viscosity and/or high cost and can lead to Li-ion cells with high gas production and/or high impedance.[13,14] In 2012, Gmitter et al.[15] opened the door for EC-free electrolytes by mixing the selected solvent (e.g. EMC) with small amount of film forming electrolyte additive (e.g. FEC). Recently, Petibon et al. further developed this type of EC-free linear alkyl carbonate-based electrolyte which yielded Li-ion cells that could be charged to 4.4 V and demonstrated long cycle and calendar life.[16] This novel class of electrolyte demonstrated low viscosity, low cost and environmentally friendly characteristics.

In the EC-free linear alkyl carbonate electrolyte, a small amount (about 2%) of vinylene carbonate (VC) was used to passivate the graphite electrode during formation. The VC used in this way was called an "enabler" because it enabled the operation of the EC-free electrolyte in Li-ion cells. In addition to VC, Xia et al. reported that several "enablers" (e.g. fluoroethylene carbonate (FEC), difluoroethylene carbonate (DiFEC) and methylene ethylene carbonate (MEC)) could also passivate the graphite electrode and yield NMC442/graphite pouch cells that could function well up to 4.4 and 4.5 V[17]. Petibon et al. suggested that the "enabler" VC could be oxidized at high potentials, resulting in gas generation and impedance growth, when the amount of the "enabler" (VC) was too large.[16] Therefore, it is critical to optimize the amount of "enabler" used in EC-free electrolytes. The effect of different "enablers" on chemistry change insides the cells during cycling or storage also needs to be investigated.

Gas chromatography coupled with mass spectrometry (GC-MS) can measure the consumption of electrolyte additives during formation, storage or cycling.[18] In this work, different concentrations of the enablers VC, MEC, FEC and DiFEC were used in EMC-based electrolyte added to NMC442/graphite pouch cells. EC was not chosen as an enabler in these studies because it did not perform competitively at high potentials (4.4 V) compared to VC or FEC.[17] The consumption of the various enablers during formation, storage (up to 4.4 V) and cycling (up to 4.4 V) were compared. Storage, electrochemical impedance spectroscopy (EIS), gas evolution, ultrahigh precision coulometry (UHPC), long term cycling, differential voltage analysis and isothermal microcalorimetry were used to determine the optimum enabler and its optimum amount.

Experimental

1.0 M $LiPF_6$ (BASF, purity 99.94%, water content 14 ppm) in ethyl methyl carbonate (EMC) (BASF, purity 99.92%, water content < 6 ppm) was used as the control electrolyte. A conventional electrolyte: 1.0 M $LiPF_6$ in EC/ EMC (3/7 by weight, from BASF, water content was 12.1 ppm), was also used for comparison. Electrolytes with additives were formulated by dissolving 1, 2, 3, 4 or 5 wt% VC (BASF, purity > 99.8%, water content < 100 ppm), MEC[18] (BASF,

*Electrochemical Society Student Member.
**Electrochemical Society Fellow.
[z]E-mail: jeff.dahn@dal.ca

Downloaded on 2018-04-23 to IP 73.168.61.127 address. Redistribution subject to ECS terms of use (see ecsdl.org/site/terms_use) unless CC License in place (see abstract).

Table I. Summary of detailed information about the electrode materials in each of the NMC442/graphite pouch cells. Each pouch cell contained 0.9 g of electrolyte. The cells were balanced for 4.7 V operation, but only used to 4.4 V.

	NMC442	Artificial Graphite
Supplier	Umicore (Korea)	Kaijin (China)
Specific Surface Area (m^2/g)	0.38 ± 0.03	1.5 ± 0.03
Mass (g)	0.96 ± 0.02	0.88 ± 0.02
Composition	96% NMC442 + 2% carbon black + 2% polyvinylidene fluoride (PVDF)	96% graphite + 2% carbon black + 2% carboxymethyl cellulose-styrene-butadiene rubber

detailed information was not provided), FEC (BASF, purity 99.94%), or DiFEC (> 99.5%, HSC Corporation, China).

Pouch cells.—Dry (no electrolyte) NMC111/graphite (220 mAh) and NMC442/graphite pouch cells (240 mAh) balanced for 4.7 V operation were obtained from Li-Fun Technology (Xinma Industry Zone, Golden Dragon Road, Tianyuan District, Zhuzhou City, Hunan Province, PRC, 412000). Table I summarizes the detailed information about the electrode materials in each of these NMC442/graphite pouch cells.

All pouch cells were vacuum sealed without electrolyte in a dry room in China and then shipped to our laboratory in Canada. Before electrolyte filling, the cells were cut just below the heat seal and dried at 80°C under vacuum for 12 hours to remove any residual water. Then the cells were transferred immediately to an argon-filled glove box for filling and vacuum sealing. All the pouch cells were filled with 0.9 g of electrolyte. After filling, cells were vacuum-sealed with a compact vacuum sealer (MSK-115A, MTI Corp.). Then cells were placed in a temperature box at 40. ±0.1°C where they rested at 1.5 V for 24 hours to allow for completion of wetting before formation. During formation all the cells were charged from 1.5 V to 3.5 V at a current corresponding to C/20 and then degassed and charged from 3.5 V to 4.2 V (cells for UHPC and calorimetry tests) or 4.4 V. Degassing means cells were opened and re-sealed under vacuum (−90 kPA gauge pressure) in the glove box to remove gas created during the formation of the SEI layers on the electrodes.

Electrochemical impedance spectroscopy.—EIS measurements were conducted on NMC111/graphite and NMC442/graphite pouch cells before and after UHPC testing, storage testing and long-term charge-discharge cycle testing. Cells were charged or discharged to 3.8 V before they were moved to a 10. ±0.1°C temperature box. Alternating current (AC) impedance spectra were collected with ten points per decade from 100 kHz to 10 mHz with a signal amplitude of 10 mV. A Biologic VMP-3 was used to collect this data.

Charge-discharge cycling tests.—All the cells were prepared for long-term cycling at 40. ±0.1°C. The cells were charged and discharged at 80 mA (C/2.5) between 2.8 and 4.4 V with constant current - constant voltage (CCCV) mode using a Neware (Shenzhen, China) charger system. The cutoff current for CCCV mode was 10 mA (C/20). All pouch cells were cycled with external clamps[7] to ensure a firm stack pressure of about 25 kPa even if gas was produced during cycling. The gas, if produced, was forced to the edges of the pouch due to the action of the clamps.

Ex-situ gas measurements.—*Ex-situ* (static) gas measurements were applied to measure gas evolution during formation, storage and cycling. The measurements were made using Archimedes' principle with cells suspended from a balance while submerged in a beaker of de-ionized "nanopure" water (18 MΩ) at 20. ±1°C. The changes in the weight of the cell suspended in the water, before and after testing are directly related to the volume changes by the change in the buoyant force. The change in mass of a cell (actually the weight, but recorded by a balance as mass), Δm, suspended in a fluid of density, ρ, is related to the change in cell volume, Δv, by

$$\Delta v = -\Delta m/\rho \quad [1]$$

Storage tests.—A Maccor series 4000 cycler was used to prepare the cells for the storage tests. Cells after formation were cycled between 2.8 V and 4.4 V twice with a current of 10 mA (C/20). Then the cells were held at 4.4 V for 24 hours and then were transferred to the storage system. The open circuit voltage of the cells was monitored automatically for 1 second every 6 hours for a total storage time of 500 h at 40.°C.[19]

GC-MS tests.—The extraction of the electrolyte components from the cell jelly roll followed the procedure described by Petibon et al.[18] In this method, dichloromethane was used as the solvent to extract the electrolyte from the jelly rolls of pouch cells. Then the extracted sample was filtered and put in a mixture of dichloromethane:water (100:1 wt/wt) to remove damaging chemicals such as PF_5 and HF which reside in the aqueous phase. A sample from the organic phase was then injected into the GC-MS. A detailed description of the GC-MS setup can be found in Reference 18.

Isothermal microcalorimetry tests.—The formed cells were cycled four times between 2.8 V and 4.2 V at 10 mA (∼C/20) to ensure well formed SEI layers before calorimetry measurements. Cells were then transferred into a TAM III Microcalorimeter (TA Instruments) at 40.00°C where the temperature was kept stable to ±0.0001°C. Cells were connected to a Maccor series 4000 charger (Maccor Inc.) for charge and discharge while in the microcalorimeter. All specifications and information regarding microcalorimetry calibration, cell connections, and operation procedures can be found in Reference 21. Heat flow measurements were recorded to an accuracy of ±1.0 μW and the baseline drift over the course of the experiments did not exceed ± 0.5 μW. After 24 hours of temperature stabilization in the calorimeter, cells were charged and discharged at 1 mA (≈ C/200) between 3.9 V and a sequence of upper cutoff voltages: 4.2 V, 4.3 V (twice), 4.4 V (twice), and again to 4.2 V (twice).

UHPC Tests.—Both formed NMC111/graphite and NMC442/graphite pouch cells underwent UHPC cycling between 2.8 V and 4.2 V at C/20, 40°C for 16 cycles. Since a power failure interrupted the test, extended cycling was done to ensure the coulombic efficiency (CE) was stable. The UHPC allows the CE and charge-end-point capacity slippage to be measured with great accuracy and relevant interpretation can be found in Reference 22.

Results and Discussion

Figure 1 shows the differential capacity vs. cell voltage of NMC442/graphite pouch cells filled with 1 M $LiPF_6$ in EMC and with 1 M $LiPF_6$ in EMC with different concentrations (from 1% to 5% by weight) of enablers: (a) VC, (b) MEC, (c) FEC and (d) DiFEC during the formation charge to 3.5 V at 40°C with a current corresponding to C/20. Data for two cells of each type, to demonstrate reproducibility, are shown. Cells with 1 M $LiPF_6$ in EMC and no enabler showed a large peak in the differential capacity plot at around 3.1 V. This results from the reduction of EMC on the surface of graphite. Adding enablers to the electrolyte suppressed this peak, indicating that the reduction of these enablers produced a good passivation layer which prevented EC reduction. The passivation of graphite is evidenced by the presence of small differential capacity peaks at around 2.8 V, 2.3 V, 2.5 V and 2.3 V for VC, MEC, FEC and DiFEC, respectively. In panel (d), a cell with 1% DiFEC still shows a substantial peak corresponding to EMC

Downloaded on 2018-04-23 to IP 73.168.61.127 address. Redistribution subject to ECS terms of use (see ecsdl.org/site/terms_use) unless CC License in place (see abstract).

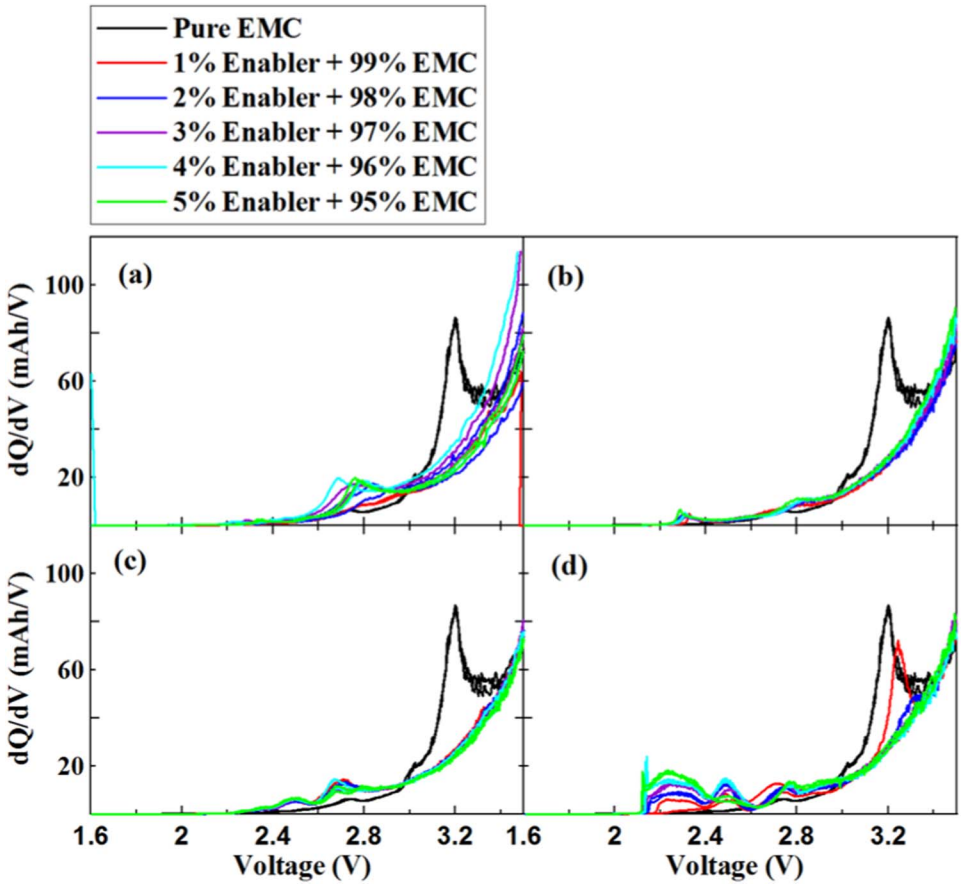

Figure 1. dQ/dV vs. voltage for NMC442/graphite pouch cells with 1 M $LiPF_6$ EMC electrolyte or 1 M $LiPF_6$ EMC containing different amounts of "enablers" as indicated during formation at 40°C with a current corresponding to C/20. (a) the enabler is VC, (b) MEC, (c) FEC and (d) DiFEC. Data for two cells of each type is shown in each panel to demonstrate reproducibility.

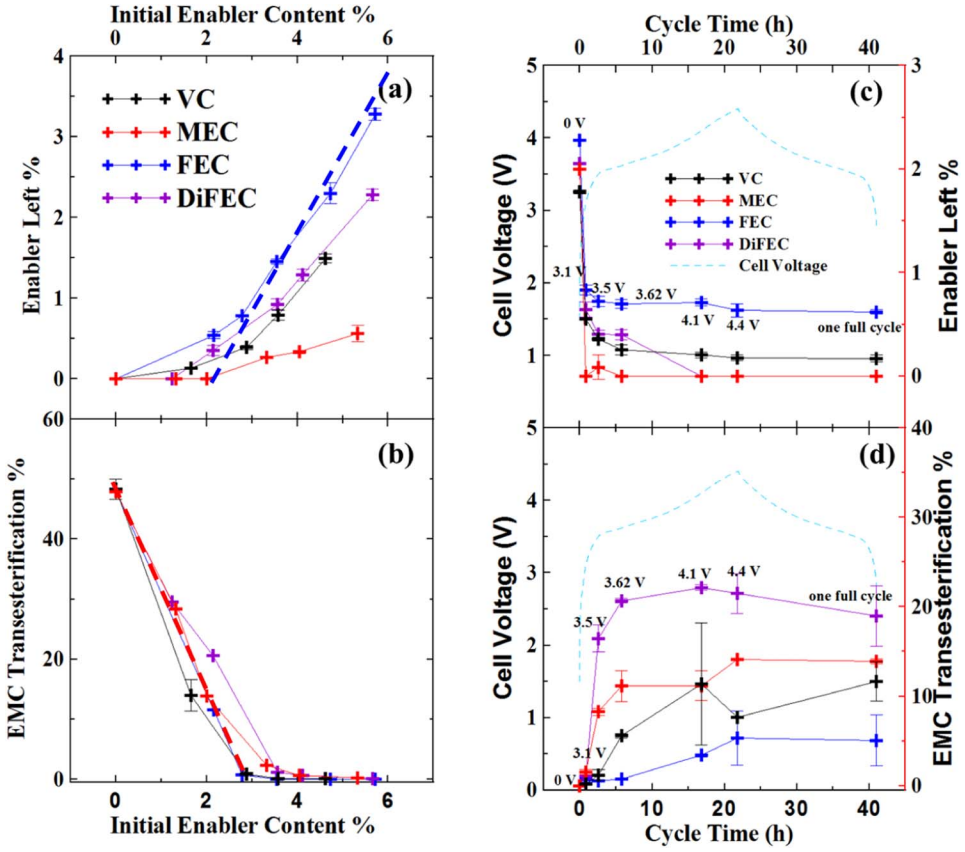

Figure 2. Amount of enabler left (a) and % EMC trans-esterification (b) vs. initial enabler content in NMC442/graphite pouch cells that underwent their first full (formation) cycle between 2.8–4.4 V at 40°C, C/20. The blue dashed line in Figure 2a is a line of slope = 1 and the same line is shown in Figures 10a and 10c. The red dashed line in Figure 2b is a guide to the eye and the same line is shown in Figures 10b and 10d. c) shows the amount of enabler left and % EMC trans-esterification (d) vs. time during the first cycle at 40°C in NMC442/graphite pouch cells initially filled with 1 M $LiPF_6$ EMC electrolyte containing ~2% enabler.

Downloaded on 2018-04-23 to IP 73.168.61.127 address. Redistribution subject to ECS terms of use (see ecsdl.org/site/terms_use) unless CC License in place (see abstract).

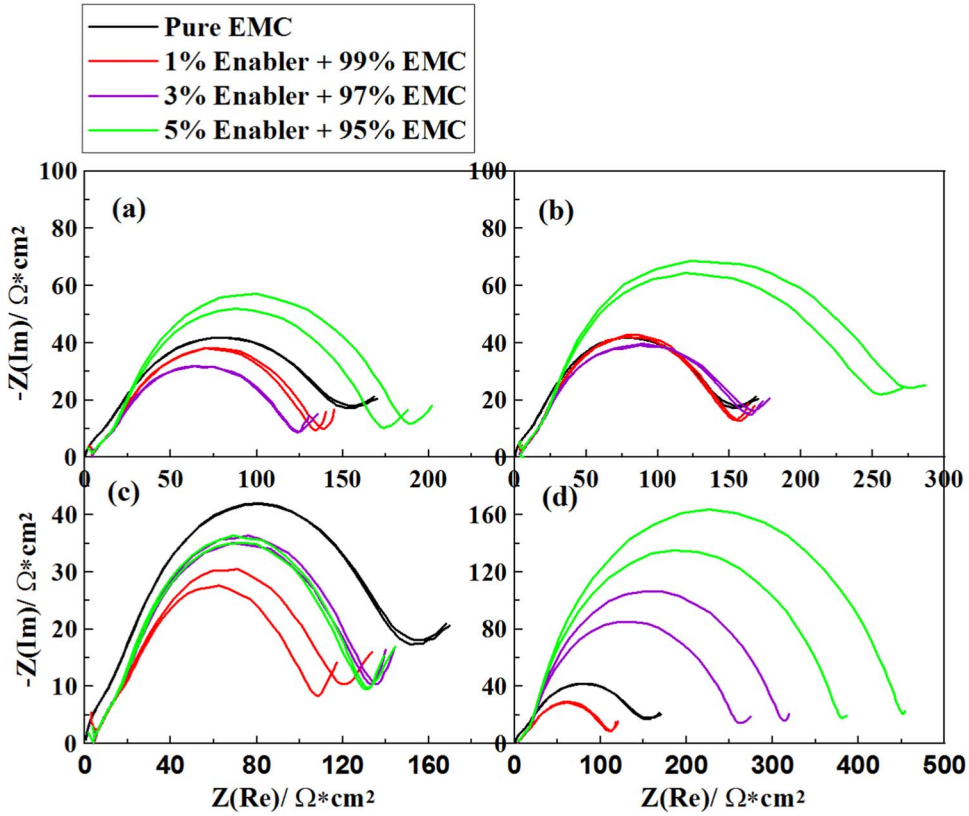

Figure 3. Nyquist plots for NMC442/graphite pouch cells with 1 M $LiPF_6$ EMC electrolyte or 1 M $LiPF_6$ EMC with different enabler content- after formation. (a) VC, (b) MEC, (c) FEC and (d) DiFEC. All the data was measured at 3.8 V and 10°C. Data for two cells of each type are presented in each panel to demonstrate reproducibility.

reduction. This shows that when the amount of enabler is too small, it may not be enough to fully passivate the graphite surface.

Figures 2a and 2b show the amount of enabler left and the percent of EMC trans-esterification after the first cycle (formation) as a function of the initial enabler content of cells that underwent formation at 40°C with a current of C/20 up to 4.4 V. The dashed blue line in Figure 2a is a line of slope 1. Comparing the data for cells with FEC in Figure 2a to the dashed blue line shows that only 2% FEC was consumed during formation even if the initial FEC content was 3, 4 or 5%. By contrast when MEC is used, the amount of MEC consumed increases with the initial MEC content, since only about 0.5% MEC is left when the initial MEC content was 5%. VC and DiFEC show intermediate behavior between FEC and MEC where some additional VC and DiFEC beyond 2% are consumed as the initial loading increases. This will have an impact on the cell as will be shown later. Figure 2b shows the percentage of EMC that underwent trans-esterification producing dimethyl carbonate (DMC) and diethyl carbonate (DEC).[23,24] The presence of lithium alkoxides caused by the reduction of linear alkyl carbonates causes these trans-esterification reactions. Therefore, when trans-esterification of EMC occurs it is a signal that EMC was reduced at the graphite negative electrode during formation. The presence or absence of DMC and DEC allows one to determine how well the graphite has been passivated by the products of the reduction of the enabler. Figure 2b shows that EMC trans-esterification is eliminated when the initial enabler content is more than a certain amount, generally about 3%. Figure 2b shows that the minimum amount of enabler required to passivate the graphite surface and prevent substantial EMC reduction should be about 3% (by weight) for the type of cell used in this study.

In order to explore the consumption of the enablers during the formation process itself, Figures 2c and 2d show the amount of enabler remaining and the percentage of EMC trans-esterification as a function of time during formation, respectively. The experiments described in Figures 2c and 2d were made with an initial enabler content of 2% (by weight). Figures 2c and 2d suggest that FEC is the most effective enabler since the least FEC is consumed and the amount of EMC undergoing trans-esterification is the smallest when FEC is used. By contrast, at a 2% loading it appears that DiFEC is the least effective enabler (on a percent weight basis) as it is totally consumed and 20% of EMC still undergoes transesterification. Figures 2c and 2d show that most of the enabler was consumed before 3.5 V and the amount of EMC undergoing trans-esterification roughly stabilizes after 3.5 V suggesting that the enablers were reduced on the graphite surface early in the formation cycle.

Based on Figure 2, three enabler contents were chosen for study using electrochemical impedance spectroscopy (EIS), storage and long-term cycling to compare the impact of different enabler content. The loadings chosen were as follows: 1% (insufficient amount), 3% (in the optimal range based on Figure 2) and 5% (possibly too much in the cases of VC, MEC and DiFEC based on Figure 2a). Figure 3 shows Nyquist plots measured after formation for NMC442/graphite pouch cells containing 1 M $LiPF_6$ in EMC and 1 M $LiPF_6$ in EMC with different enabler contents: (a) VC, (b) MEC, (c) FEC and (d) DiFEC. The impedance spectra were measured at 3.8 V and at 10.0°C. The diameter of the semi-circle arises from the sum of the charge-transfer resistances and the transport of lithium ions through the SEI layers at both the positive and negative electrodes. In this work, the diameter of the semicircle is called R_{ct}. [Note: The interpretation of the impedance spectra in this work follows that of Atebamba et al.[25] and R_{ct} is regarded as the main contribution to the diameter of the semi-circle]. In the case of VC, MEC and DiFEC, the diameter of the semicircle increases dramatically when 5% enabler is used, while with FEC it does not. According to Figure 2a the amount of enabler consumed increases for VC, MEC and DiFEC when the initial enabler content

Downloaded on 2018-04-23 to IP 73.168.61.127 address. Redistribution subject to ECS terms of use (see ecsdl.org/site/terms_use) unless CC License in place (see abstract).

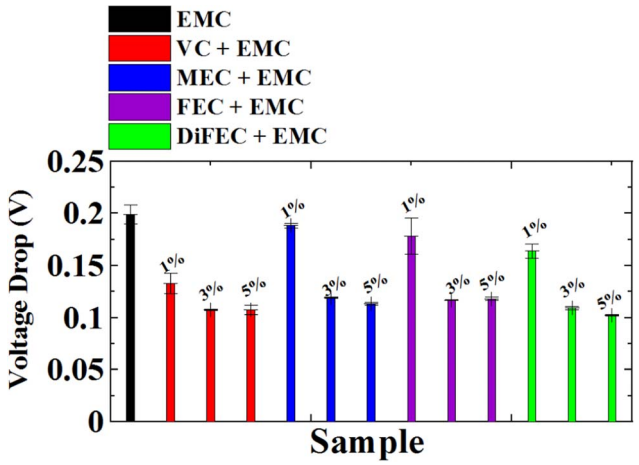

Figure 4. Summary of voltage drop during 500 hour storage at 4.4 V and 40°C for NMC442/graphite pouch cells with 1 M $LiPF_6$ EMC electrolyte or 1 M $LiPF_6$ EMC with different enabler content as indicated.

increased beyond 3% which would thicken the negative electrode SEI layer causing impedance increase as observed in Figure 3. In the case of FEC, Figure 2a shows that only 2% FEC is consumed even if 3, 4 or 5% FEC is initially loaded in the cell. This is consistent with the results in Figure 3 which show the impedance of the cells with FEC does not increase with FEC loading for the cells with 3% and 5% FEC.

Figure 4 shows a summary of voltage drop of NMC442/graphite pouch cells containing 1 M $LiPF_6$ in EMC and 1 M $LiPF_6$ in EMC with different enabler contents: VC, MEC, FEC and DiFEC during the storage test at 40°C. Two cells were measured for each data point and the error bars in Figure 4 are the difference between the two results. The voltage drop during the storage test indicates the occurrence of parasitic reactions at the surface of the positive electrode. We believe the lithium alkoxides created by EMC reduction are responsible for the rapid self-discharge as they can be involved in shuttle type reactions. Compared to the cells with 1 M $LiPF_6$ in EMC and the cells with 1% enabler, the cells with 3% or 5% enabler show a significantly smaller voltage drop. Based on Figure 2b, there were little to no Li alkoxides present in the electrolyte when the enabler content was 3% or greater so the self-discharge during storage should be less severe, as observed. For each enabler, there is little or no difference between cells with 3% or 5% enabler based on the storage data. In addition, the choice of enabler does not affect the voltage drop during storage when the enabler content is 3% or 5%.

Figures 5a–5d show the capacity versus cycle number for NMC442/graphite pouch cells containing 1 M $LiPF_6$ in EC/EMC (3/7), 1 M $LiPF_6$ in EMC and 1 M $LiPF_6$ in EMC with different enabler contents: (a) VC, (b) MEC, (c) FEC and (d) DiFEC during CCCV cycling up to 4.4 V at 40°C with a current that corresponded to C/2.5. The constant voltage cutoff current corresponded to C/20. Figures 5e–5h show the difference between the average charge and the average discharge potential (ΔV) vs. cycle number corresponding to the cells shown in Figures 5a–5d, respectively. The value of ΔV is a measure of the polarization in the cells.[26] Cells with 1 M $LiPF_6$ in EC:EMC performed poorly in this test. Compared to cells with 1 M $LiPF_6$ in EMC and cells with 1% enabler, cells with 3% or 5% enabler show better capacity retention and smaller polarization growth during long-term cycling. Figures 5g and 5h show that FEC and DiFEC control polarization growth during cycling better than VC and MEC. Even with a 1% loading of FEC or DiFEC, the polarization of the cells after 200 cycles is comparable to that of cells with a 5% loading of VC or MEC.

Differential voltage analysis was performed on NMC442/graphite pouch cells after long term cycling to determine the reason for the capacity loss and to compare differences between various enablers with different concentrations. Loss of Li inventory due to SEI growth and repair as well as loss of active material are the possible causes of low rate capacity loss. Impedance growth can reduce cell capacity at high rate. Dahn et al.,[27] among others[28,29] showed that differential voltage analysis allows the active masses of both electrodes and the relative capacity slippages of each electrode to be determined. In this work, these parameters were obtained using reference differential voltage curves measured in NMC442/Li and graphite/Li half cells for fit dV/dQ vs. Q of the full cells.

Figure 6a shows the measured Li-ion cell (after 200 cycles of CCCV cycling shown in Figure 5) voltage vs. capacity curve at C/20,

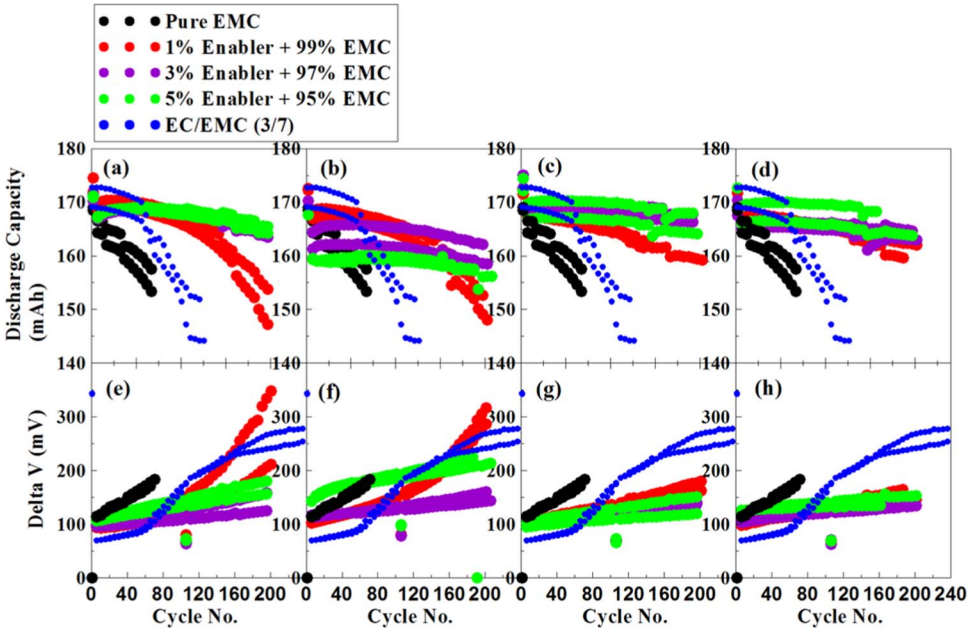

Figure 5. Discharge capacity (a) to (d) and cell polarization (e) to (h) vs. cycle number for NMC442/graphite pouch cells with 1 M $LiPF_6$ EMC electrolyte or 1 M $LiPF_6$ EMC with different enabler content during long term CCCV cycling at 40°C between 2.8 V and 4.4 V using currents corresponding to C/2.5. A constant voltage step at the top of charge was applied until the current dropped below C/20. (a), (e) VC; (b), (f) MEC; (c), (g) FEC and (d), (h) DiFEC. Data for two cells of each type are included in each panel to demonstrate reproducibility.

Downloaded on 2018-04-23 to IP 73.168.61.127 address. Redistribution subject to ECS terms of use (see ecsdl.org/site/terms_use) unless CC License in place (see abstract).

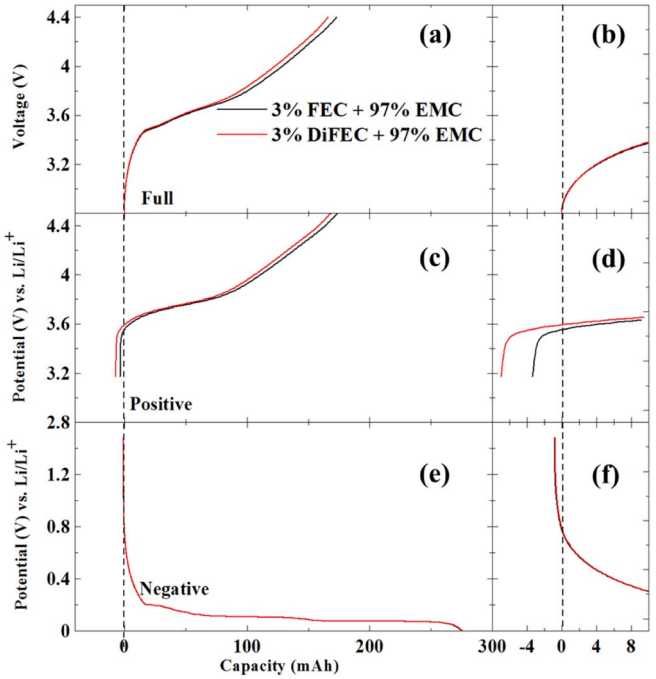

Figure 6. (a) Measured NMC442/graphite cell (after long term cycling shown in Figure 5) V(Q) curves cycled at C/20 at 40°C. Extracted $V_p(Q)$ (b) and $V_n(Q)$ (c) curves, respectively, from the dV/dQ analysis software. These $V_p(Q)$ and $V_n(Q)$ curves are the potentials of the positive electrode (NMC442) and negative electrode (graphite) vs. Li/Li^+ and these curves are aligned along the capacity axis just as they are in the full cell. The right inset panels (b), (d) and (f) show an expanded view of the region near Q = 0 for panels (a), (c) and (e), respectively.

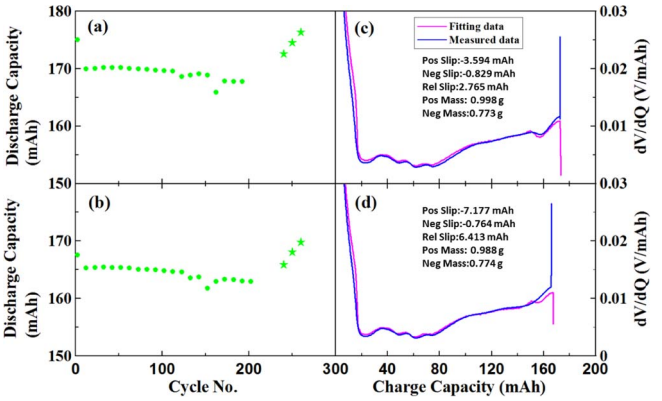

Figure 7. Discharge capacity vs. cycle number (a and b, for NMC442/graphite pouch cells with 1 M $LiPF_6$ EMC containing 3% FEC or 3% DiFEC, respectively, during CCCV long term cycling at 40°C between 2.8 V and 4.4 V with currents corresponding to C/2.5. A constant voltage step at the top of charge was applied until the current dropped below C/20. The star-shaped points in each panel are the low rate cycling data collected after the long term cycling. The first one was measured at C/20, the second one was measured at C/40 and the third one was measured at C/80. Panels c and d show the differential voltage vs. capacity curve and the fitted curve for the cells in panels a) and b) after 200 cycles. A C/20 charge curve collected after 200 cycles was used for the fitting.

40°C. Figures 6c and 6e show the potential vs. capacity curves for the fitted positive and negative electrodes, respectively. Figures 6b, 6d and 6f are enlargements of Figures 6a, 6c and 6e, respectively, near the zero of the capacity axis. Cells with 1 M $LiPF_6$ in EMC containing 3% FEC or 3% DiFEC are selected as examples to discuss here. The electrode masses and slippages used in Figure 6 and Figures 7c and 7d are those that gave the best fits between the measured and calculated dV/dQ vs Q curves. The point Q = 0 indicated by the dashed line in Figure 6 is taken as the point where the full Li-ion cell reaches the fully discharged state. The positive or negative electrode slippage can be negative or positive compared to Q = 0 as shown in Figures 6d and 6f. The relative slippage is very small indicating that very little capacity loss had occurred by loss of Li inventory at the negative electrode. This is consistent with the data in Figures 7a and 7b where the low rate C/20 cycle at the beginning of the testing (cycles 1 and 2) has virtually the same capacity as the C/20 cycles after 200 cycles (plotted as the star-shaped data points at cycle 240, for clarity). Therefore, Figures 6 and 7 show that the reason for capacity loss in these cells with 3% FEC or 3% DiFEC is impedance growth. Although not shown, the same conclusions can be made about all cells with 3% and 5% enabler. The low rate C/20 capacity after 200 cycles is virtually the same as the low rate C/20 capacity during cycles 1 and 2. Thus, the capacity fade shown in Figures 5c and 5d is predominantly due to impedance growth.

The situation is more complex for the capacity fade of cells with 1 M $LiPF_6$ in EMC and for cells with 1% enabler in 1 M $LiPF_6$ in EMC shown in Figures 5a and 5b. In those cases the low rate (C/20) cycles collected after 200 cycles did not match the capacity of cycles 1 and 2 at C/20 (see Figure S1 in the supplementary information). Even when the same cells were tested at C/40 and C/80 after 200 cycles, their capacities were still about 5 to 10% less than their initial low rate capacity (see Figure S1 in the supplementary information). This suggests loss of Li inventory as well as impedance growth for the cells with no enabler or 1% enabler. This is consistent with a poorly passivated negative electrode as shown in Figures 2a and 2b for cells with no enabler or 1% enabler.

Figure 8 shows a summary of the impedance (R_{ct}, diameter of the EIS semicircle) of NMC442/graphite pouch cells containing 1 M $LiPF_6$ in EMC or 1 M $LiPF_6$ in EMC with different enabler (VC, MEC, FEC or DiFEC) contents. Data are shown for R_{ct} collected after formation (Figure 3), after storage (Figure 4) and after long-term CCCV cycling (Figure 5). Cells using FEC as the enabler showed the lowest R_{ct} compared all other cells, and R_{ct} remained small even when the FEC content in the electrolyte was initially 5%. By contrast, when VC, MEC or DiFEC were used, R_{ct} increased with enabler content. Cells with 3% FEC or 5% FEC showed similar values of R_{ct} after formation, after storage and after CCCV cycling. Again, FEC appears to be the best choice among these four enablers.

Figure 9 shows the summary of the gas production in NMC442/graphite pouch cells containing 1 M $LiPF_6$ in EMC and 1 M $LiPF_6$ in EMC with different enabler contents (VC, MEC, FEC or DiFEC) after long-term CCCV cycling to 4.4 V at 40°C (a), after storage (4.4 V, 500 h, 40°C) (b) and after formation (c). Figure 9 is very interesting. During formation, cells with only 1% enabler produced more gas than those with 3% or 5% enabler, most likely due to poorly passivated graphite. During storage and CCCV cycling, cells with 5% VC, 5% MEC or 5% DiFEC produced more gas than those with 3% of the same enablers, presumably due to oxidation of excess enabler. During storage and CCCV cycling, cells with 1% MEC, 1% FEC and 1% DiFEC produced more gas than those with 3% of the same enablers presumably due to poor passivation of the graphite and resulting EMC reduction. Cells that had 3% MEC, 3% FEC, 5% FEC and 3% DiFEC showed very little gas generation in these tests presumably because the graphite was well passivated and, in the cases of MEC and DiFEC, little excess enabler remained to be oxidized at the positive electrode. In the case of FEC, excess FEC above 3% did not lead to gassing at 40°C presumably due to the oxidative stability of FEC.

Figures 10a and 10c show the amount of enabler left in the electrolyte after storage (10a) and long term CCCV cycling (10c) as a function of the initial enabler content. These data should be compared to the data in Figure 2a which showed the amount of enabler left after formation. The blue dashed lines in Figures 2a, 10a and 10b are the same and can be used to see that the concentration of FEC in the

Downloaded on 2018-04-23 to IP 73.168.61.127 address. Redistribution subject to ECS terms of use (see ecsdl.org/site/terms_use) unless CC License in place (see abstract).

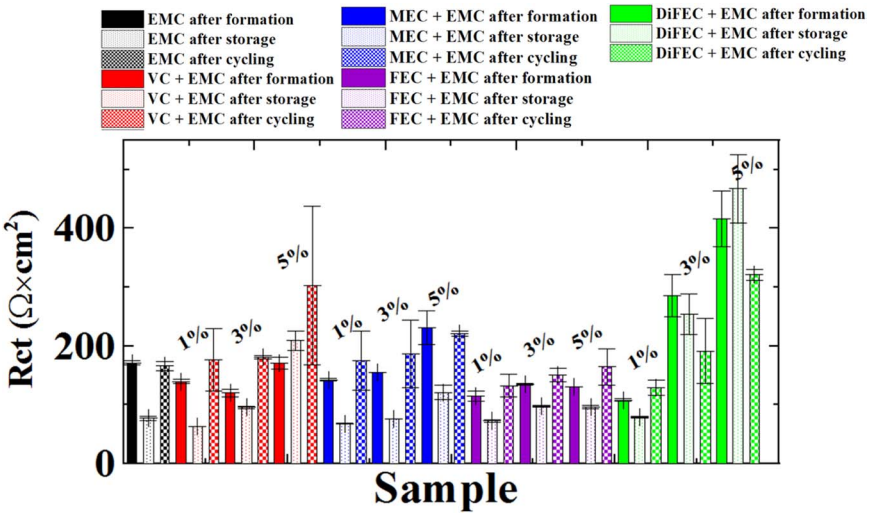

Figure 8. A summary of the impedance results for NMC442/graphite pouch cells with 1 M $LiPF_6$ in EC/EMC (3/7), 1 M $LiPF_6$ in EMC or 1 M $LiPF_6$ in EMC with different enabler content as indicated after formation (40°C, C/20), after 500 h storage (4.4 V, 40°C) and after ~200 CCCV cycles (2.8 – 4.4 V, 40°C, C/2.5). All the EIS data was measured at 3.8 V and 10°C. The data shown is the average of two cells and the error bars represent the range of the measurements.

electrolytes containing 3% or 5% FEC was virtually unchanged after storage or cycling compared to the concentration after formation. By contrast, the concentration of all other enablers decreased during storage and during long term cycling. Figures 10b and 10d show the amount of EMC trans-esterification that occurred after storage (10b) and after long term cycling (10d) as a function of the initial enabler content. The red dashed lines in Figures 2b, 10b and 10d are the same and can be used to see that the amount of transesterification increased dramatically during storage and cycling for all cells that initially had 1% of enabler added. This, again, shows that 1% enabler is insufficient to passivate the graphite electrode. However, with an initial loading of 3% or 5% enabler, the percentage of EMC trans-esterification did not increase during storage (500 hours) or long-term cycling (~200 cycles). This suggests the formation of a robust solid electrolyte interphase (SEI) on the negative electrode when the enough enabler was added initially.

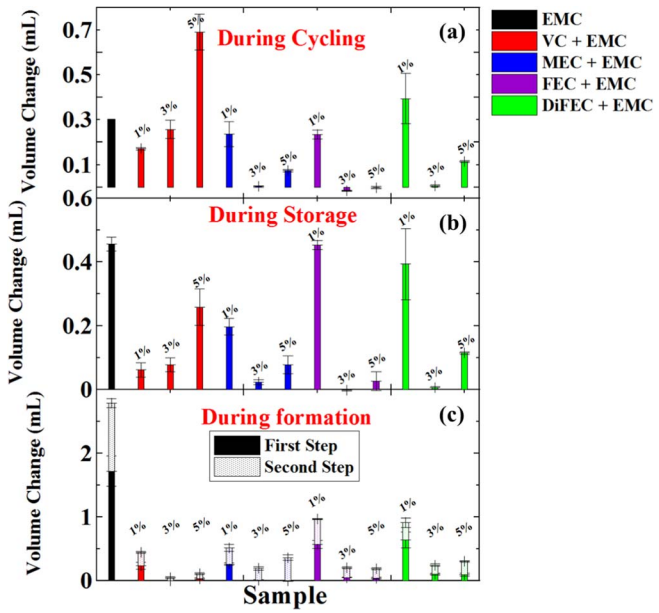

Figure 9. A summary of the gas volumes in NMC442/graphite pouch cells with 1 M $LiPF_6$ EMC electrolyte or 1 M $LiPF_6$ EMC with different enabler content as indicated: (a) after ~200 CCCV cycles (2.8 – 4.4 V, 40°C, C/2.5), (b) after 500 h storage (4.4 V, 40°C) and (c) after formation (40°C, C/20). All the data was measured at 1 atm. and 20°C. The data shown is the average of two cells and the error bars represent the range of the measurements.

Isothermal microcalorimetry has been used in the previous studies to investigate the parasitic heat flow of high voltage reactions in lithium ion cells using various charge-discharge methods.[30–32] Downie et al. showed that at sufficiently low currents, the parasitic heat flow may be calculated as the average of heat flow during charge and discharge at each voltage point.[33] In this work, the parasitic heat flow was calculated as the average heat flow at each voltage point during charge-discharge cycles. Cells were cycled at 1 mA (~C/200) between 3.9 V and upper cutoff voltages between 4.2 V and 4.4 V at 40.00°C.

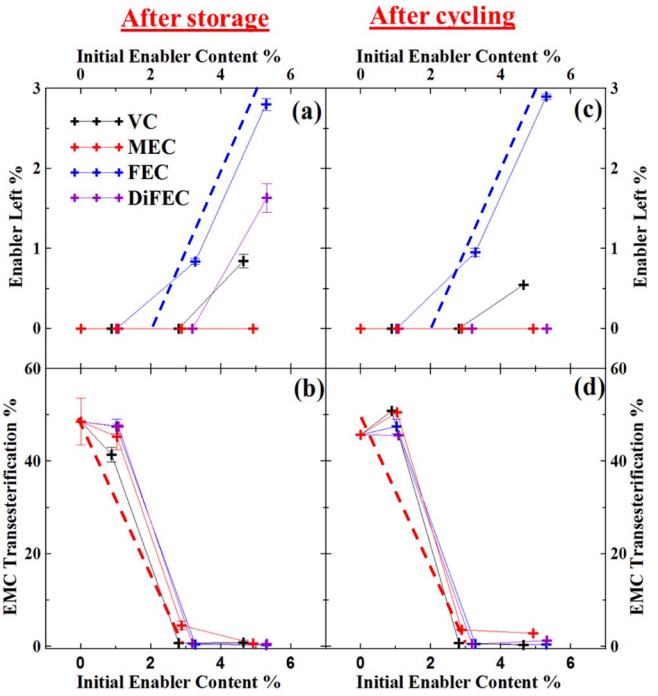

Figure 10. Amount of enabler left (a) and % EMC trans-esterification (b) vs. initial enabler content in NMC442/graphite pouch cells that underwent 500 h storage at 40°C, 4.4 V; amount of enabler left (c) and % EMC trans-esterification (d) vs. initial enabler content in NMC442/graphite pouch cells that underwent ~200 CCCV cycles (2.8 – 4.4 V, 40°C, C/2.5). A constant voltage step at the top of charge was applied until the current dropped below C/20. The data shown is the average of two cells and the error bars represent the range of the measurements. The blue dashed and red dashed lines are the same lines shown in Figure 2 and are reproduced here so data from Figure 2 and 10 can be compared.

Downloaded on 2018-04-23 to IP 73.168.61.127 address. Redistribution subject to ECS terms of use (see ecsdl.org/site/terms_use) unless CC License in place (see abstract).

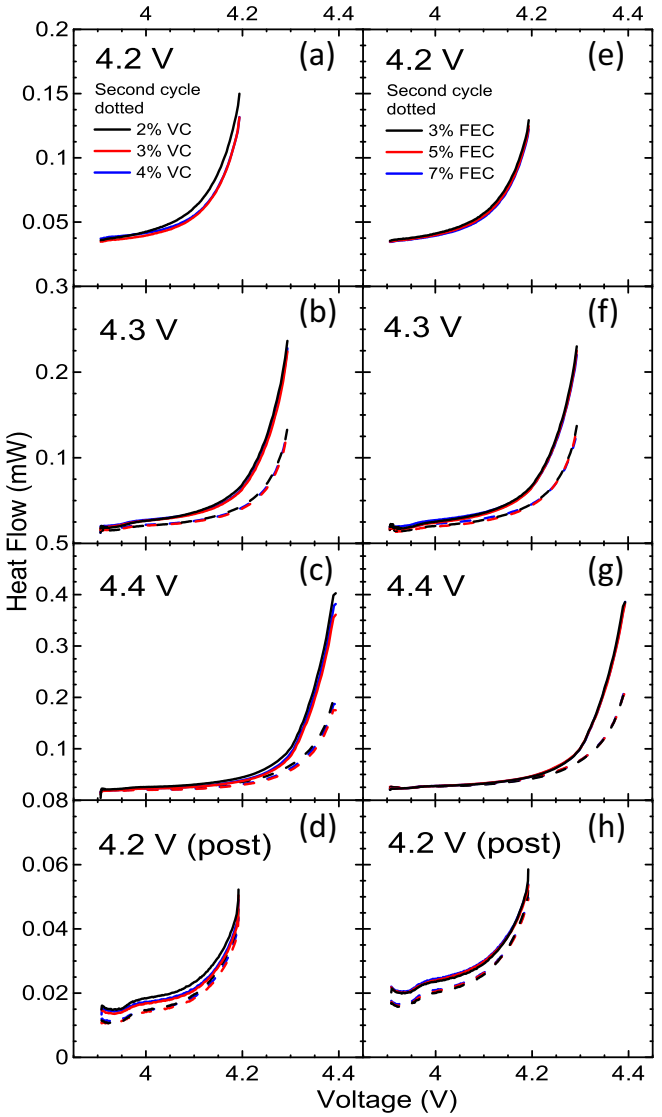

Figure 11. The calculated parasitic heat flow of NMC442/graphite cells with 1 M $LiPF_6$ EMC electrolyte containing different amounts of VC (left panel) or FEC (right panel). The rows in Figure 11 follow a chronological order, ie. the top row was performed first. Cycles were between 3.9 V and 4.2 V (a,e), 4.3 V (b,f), 4.4 V (c,g) and 4.2 V (d,h) (post high voltage) at 1 mA at 40°C. Each measurement after the first step to 4.2 V was performed twice in order to determine to which extent the exposure to high voltage had damaged the electrolyte, and is shown as a dotted line.

The isothermal calorimetry studies were used to try to optimize the amount of VC or FEC to use as enablers.

Figure 11 shows the calculated parasitic heat flow versus potential of cells containing different amounts of VC or FEC in 1 M $LiPF_6$ EMC electrolyte. The left column shows results for cells containing VC and the right column shows cells with FEC. The rows in Figure 11 follow a chronological order, ie. the top row showing a cycle to 4.2 V, Figures 11a and 11e, were performed first. Cycles to 4.3 V, 4.4 V and 4.2 V (post high voltage) shown in Figures 11b,11f,11c,11g and 11d,11h respectively, were performed twice in order to determine to which extent the exposure to high voltage had damaged the electrolyte. Ideally, electrolytes would recover from high voltage exposure and parasitic heat flow would decrease in subsequent cycles. The second cycle to each voltage is shown as a dashed line, and in every case electrolytes exhibited parasitic heat flow lower than that of the first cycle. Figures 11c and 11d show a slight advantage of 3% and 4% VC over 2% VC. Figures 11a,11b, 11e, 11f, 11g and 11h show that it

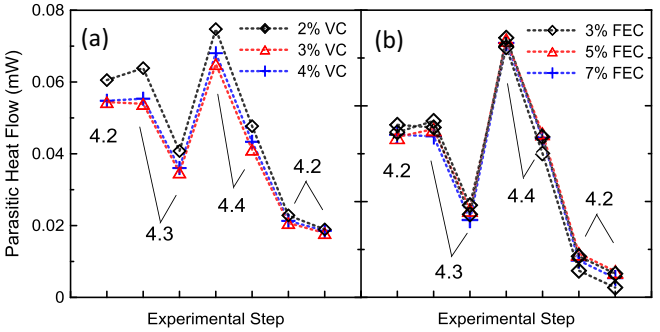

Figure 12. The mean parasitic heat flow during each cycle shown in Figure 11 for cells with 1 M $LiPF_6$ EMC electrolyte containing VC (a) or FEC (b), respectively.

is very hard to distinguish an enabler concentration that gives a clear "winner" (i.e. the lowest parasitic heat flow) in these sensitive tests.

The average parasitic heat flow during each cycle provides a convenient method of comparison, and is shown in Figures 12a and 12b for VC and FEC-containing cells, respectively. In cells containing VC, a small improvement in parasitic heat flow was observed when increasing the amount of VC from 2% to 3% by weight, and no further improvement was seen when 4% VC was added. The addition of larger amounts of VC also increased the impedance of cells after cycling (see Figure S3 in the supplementary information), so 3% VC is probably close to the optimal amount. Figure 12b shows that no significant improvements in parasitic heat flow were seen with the addition of more than 3% FEC. A comparison between Figures 12a and 12b shows that the parasitic heat flow in VC-containing cells at 4.2 V after exposure to 4.4 V is lower than that of FEC-containing cells. The parasitic reactions in these cells may not be exactly the same and may have different enthalpy of reaction so it is difficult to say whether VC or FEC-containing cells are better based on these experiments alone.

In a further attempt to determine the optimum amount of VC or FEC to use in EC-free electrolytes based on 1 M $LiPF_6$ in EMC, some NMC111/graphite and NMC442/graphite pouch cells were subjected to UHPC cycling (16 cycles) between 2.8 and 4.2 V with a current corresponding to C/20 at 40°C. As a comparison, data for similar NMC111/graphite and NMC442/graphite cells with a 1 M $LiPF_6$ in EC:EMC (3:7 wt) plus 2% VC electrolyte have been included. Figure 13 shows the significant parameters from the UHPC test: (a) coulombic efficiency (CE), (b) charge end-point capacity, (c) discharge capacity and (d) ΔV (the difference between the average charge voltage and the average discharge voltage) all plotted vs. cycle number. Test results for one cell are used as an example in each panel to show the method of determining the UHPC results in this manuscript. In panel (a), the CE values from the last five cycles (12–16 cycles) were fitted with a line to predict the CE value at cycle 16. The coulombic inefficiency (CIE) was calculated by taking CIE = 1 – CE, where CE is the value of the CE from the fitted line at cycle 16. The CIE is then divided by the time of one cycle to get CIE/hour as shown in Figure 14a. In Figures 13b, 13c and 13d, the values from the last five cycles (12–16 cycles) were fitted with a line. The slopes of the charge end-point capacity versus cycle number and the discharge capacity versus cycle number were then divided by the time of one cycle and the discharge capacity of the first cycle. These give the fractional charge end point capacity slippage per hour and the fractional capacity fade per hour, respectively. The relevant results are summarized in Figures 14b and 14c, respectively. The slope of the ΔV versus cycle number graph was divided by the time of one cycle to get the polarization growth rate as shown in Figure 14d.

In Figure 14, each data point is the average for two nominally identical cells. The error bar of plotted at each value consists of two parts: (1) the variation from cell to cell and (2) the error associated with the measured value based on quality of the fitted line to the last

Downloaded on 2018-04-23 to IP 73.168.61.127 address. Redistribution subject to ECS terms of use (see ecsdl.org/site/terms_use) unless CC License in place (see abstract).

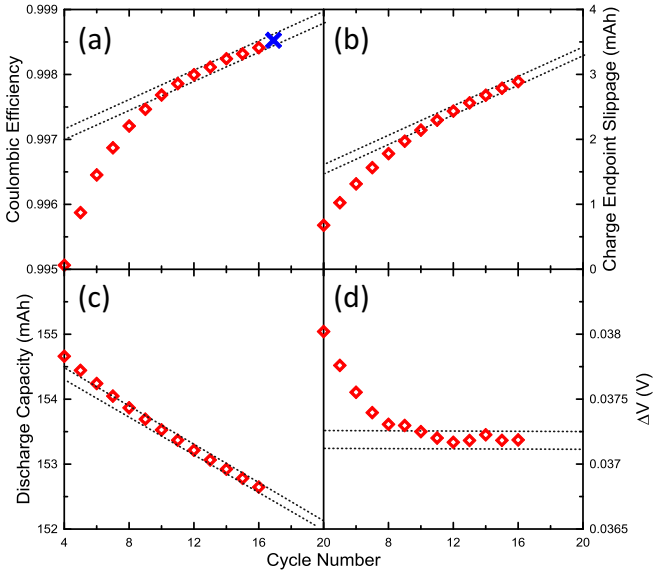

Figure 13. The typical measurables of a UHPC test including (a) coulombic efficiency (CE), (b) charge end-point capacity, (c) discharge capacity and (d) ΔV vs. cycle number. Dashed lines in each panel indicates the linear fit for the last five data points in each panel. The blue cross in panel (a) represents the predicted CE value at cycle 16 based on the linear fit.

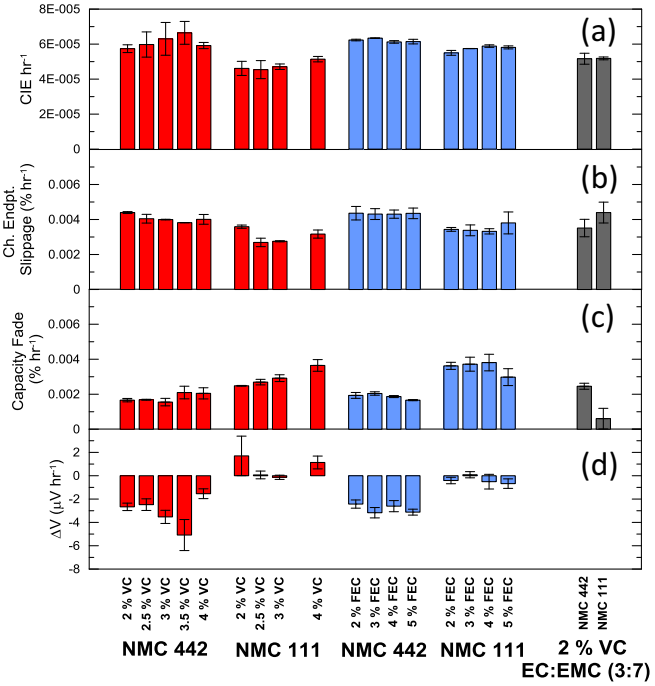

Figure 14. A summary of UHPC test results for NMC111/graphite and NMC442/graphite pouch cells filled with 1 M $LiPF_6$ in EMC plus different concentrations of VC (2%, 2.5%, 3%, 3.5%, 4%) (red) or FEC (2%, 3%, 4%, 5%) (blue) and for cells with 1 M $LiPF_6$ in EC:EMC (3:7 wt) + 2% VC (gray) during 16 cycles between 2.8 and 4.2 V with currents corresponding to C/20 at 40°C including (a) coulombic inefficiency per hour, (b) fractional charge end-point capacity slippage per hour, (c) fractional discharge capacity fade per hour and (d) increase in ΔV per hour. Each data point shown in Figure 14 is based on a linear fit to the last five cycles. The data shown is the average of two cells and the error bars were calculated as described in the text.

five points. These two contributions to the error have been combined according to standard practices in error propagation.[34]

The fractional fade per hour (Figure 14c) represents lithium loss due to SEI growth at the negative electrode while the fractional charge end-point capacity slippage per hour (Figure 14b) measures the rate of the electrolyte oxidation at the positive electrode.[22] Generally, lower fractional charge end-point capacity slippage, lower fractional fade and lower CIE lead to the cells with longer lifetime.[35] When cells were operated to 4.2 V, the concentration of FEC (from 2% to 5%) barely affected the cell performance while 4% VC led to higher capacity fade compared to other cells with smaller amounts of VC. The raw initial UHPC test data (Figure S2), impedance test results and gas evolution during UHPC cycling (Figure S3) can be found in the supplementary information. Figure S3 clearly shows that there are penalties with respect to impedance if increased amounts of VC are used. Finally, the UHPC results (Figures S2 and 14) and the isothermal microcalorimetry results (Figures 11 and 12) suggest that there is little to distinguish between cells with between 2 and 4% VC from a lifetime standpoint and between cells with 3 and 5% FEC from a lifetime standpoint. Figure 14 also shows that the EC-free electrolytes give comparable performance to 1 M $LiPF_6$ EC:EMC (3:7) + 2% VC when cells are operated to 4.2 V. The advantage of the EC-free electrolytes comes when cells are operated to 4.4 V and above as detailed in References 16 and 17.

Figure 15 shows a "radar" plot which compares the effects of selected enablers (1%, 3% and 5%) on NMC442/graphite pouch cells using "EC-free" electrolytes (a)VC (b) MEC (c) FEC and (d) DiFEC studied using GC-MS (Figure 2), EIS (Figure 3 and Figure 8), storage (Figure 4), long-term cycling (Figure 5) and cell volume change testing (Figure 9). The six axes in the radar plots represent the average of two cells. The axes consist of impedance after formation ($\Omega \times cm^2$), gas evolution during cycling (mL), fraction of enabler consumed during formation (%), voltage drop during storage (V), discharge capacity fade during cycling (%) and impedance after cycling ($\Omega \times cm^2$). Values closest to the center of the radar plot are best. The scales on the axes in Figures 15a, 15b, 15c and 15d are the same. It is clear that 3% and 5% enablers yield advantages in most aspects of cell performance (e.g. voltage drop, capacity retention, etc.) compared to 1% enabler. Figure 15 clearly shows that the choice of 3% or 5% FEC as the enabler would yield the best cells based on these metrics.

Conclusions

Electrolytes consisting of 1 M $LiPF_6$ in EMC plus a small amount of "enabler" have been demonstrated useful for NMC442/graphite pouch cells operated at high potential. The work in this paper focused on strategies for finding the best EC-free electrolyte for high voltage LIB. In addition to the selected "enablers" studied in this work, there are many more "enablers" that need to be identified and carefully tested. Studies of EC-free electrolytes have remarkable clarity because there is no EC present in the electrolyte to contribute to a complex negative electrode SEI that contains decomposition products from EC as well as from the electrolyte additives. The clear reduction peak of EMC observed during formation (Figure 1) as well as the trans-esterification of EMC which occurs when Li alkoxides are created by EMC reduction (Figure 2) allows one to easily determine when enough enabler has been added to the EC-free electrolyte to passivate the graphite negative electrode effectively. It is our opinion that such clear and remarkable data, of an almost tutorial nature, cannot be collected for electrolytes that contain EC.

In order to optimize the amount of "enabler" added to 1 M $LiPF_6$ in EMC, GC-MS was used to track the consumption of "enabler" and the trans-esterification of EMC during formation. Cells containing different initial amounts of "enabler" were systematically investigated using storage tests, EIS, long-term CCCV cycling, isothermal microcalorimetry and UHPC tests. The tools used here are very appropriate to use to understand the impact of electrolyte additives in Li-ion cells.

If the amount of "enabler" added to 1 M $LiPF_6$ in EMC was not enough (e.g. 1%), the graphite negative electrode was not passivated well, which resulted in gas production during formation, storage and cycling, rapid capacity fade and polarization increase during cycling. If the amount of "enabler" was in excess (e.g. 5%), it resulted in large impedance and gas production during storage and cycling, except in

Downloaded on 2018-04-23 to IP 73.168.61.127 address. Redistribution subject to ECS terms of use (see ecsdl.org/site/terms_use) unless CC License in place (see abstract).

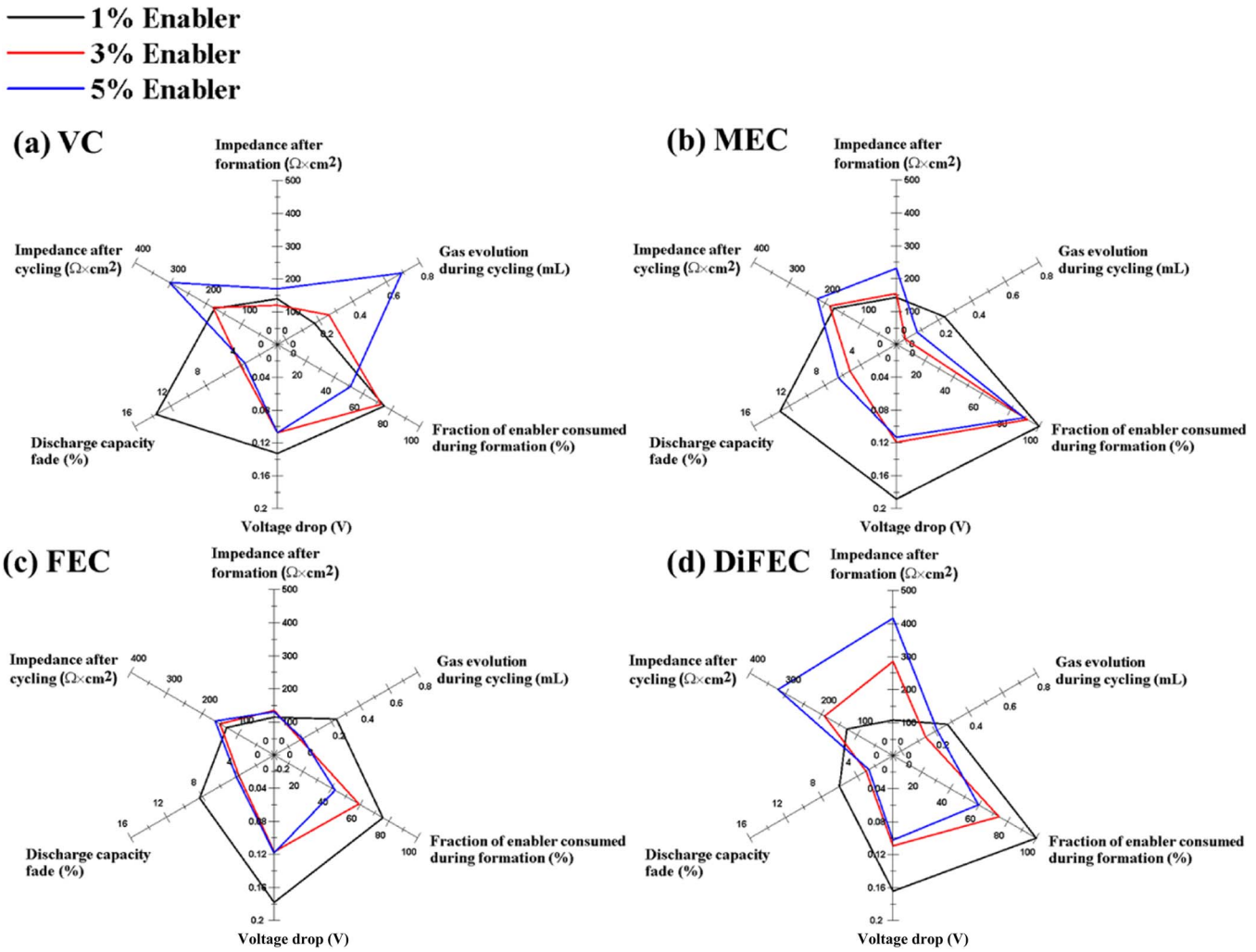

Figure 15. Radar plots summarizing the effects of selected enablers (1%, 3% and 5%) on NMC442/graphite in "EC-free" electrolyte system (a)VC (b) MEC (c) FEC and (d) DiFEC. Each data point in Figure 15 represents the average of two cells. The axes consist of impedance after formation ($\Omega \times cm^2$), gas evolution during cycling (mL), fraction of enabler consumed during formation (%), voltage drop during storage (V), discharge capacity fade during cycling (%) and impedance after cycling ($\Omega \times cm^2$). The exact initial content of the enablers (1%, 3% and 5%) has been shown in Figure 2(a). Values closest to the center of the radar plot are best.

the case of FEC. FEC was the only enabler that was only consumed to a level of about 2% during formation even if excess FEC was added which explains why the impedance did not increase when excess FEC was added. In addition, the amount of FEC in the electrolyte did not diminish during the storage and cycling tests performed here. Based on all the data and on the summary in Figure 15, cells with 3% FEC or 5% FEC in 1 M $LiPF_6$ EMC appear to be the best in the testing performed here.

Acknowledgments

The authors thank NSERC, 3M Canada for the funding of this work under the auspices of the Industrial Research Chairs program. The authors thank Dr. Jing Li of BASF for providing most of the solvents and salt used in this work. The authors thank Xiaodong Cao of HSC corporation for providing the DiFEC used in this work. S. L. Glazier and R. Petibon thank NSERC for scholarship support. Jeremy M. Peters thanks the Burgess McKittrick foundation for bursary support.

References

1. B. Dunn, H. Kamath, and J.-M. Tarascon, *Science*, **334**, 928 (2011).
2. L. Ma, K. E. Hendrickson, S. Wei, and L. A. Archer, *Nano Today*, **10**, 315 (2015).
3. M. Hu, X. Pang, and Z. Zhou, *J. Power Sources*, **237**, 229 (2013).
4. Y.-K. Sun, S.-W. Cho, S.-W. Lee, C. S. Yoon, and K. Amine, *J. Electrochem. Soc.*, **154**, A168 (2007).
5. S.-K. Hu, G.-H. Cheng, M.-Y. Cheng, B.-J. Hwang, and R. Santhanam, *J. Power Sources*, **188**, 564 (2009).
6. M. Nie, J. Xia, and J. R. Dahn, *J. Electrochem. Soc.*, **162**, A1693 (2015).
7. M. Nie, J. Xia, and J. R. Dahn, *J. Electrochem. Soc.*, **162**, A1186 (2015).
8. Z. Zhang, L. Hu, H. Wu, W. Weng, M. Koh, P. C. Redfern, L. A. Curtiss, and K. Amine, *Energy Environ. Sci.*, **6**, 1806 (2013).
9. E. Markevich, G. Salitra, K. Fridman, R. Sharabi, G. Gershinsky, A. Garsuch, G. Semrau, M. A. Schmidt, and D. Aurbach, *Langmuir*, **30**, 7414 (2014).
10. H. Duncan, N. Salem, and Y. Abu-Lebdeh, *J. Electrochem. Soc.*, **160**, A838 (2013).
11. J. Xia, J. Self, L. Ma, and J. R. Dahn, *J. Electrochem. Soc.*, **162**, A1424 (2015).
12. A. Abouimrane, I. Belharouak, and K. Amine, *Electrochem. Commun.*, **11**, 1073 (2009).
13. K. Xu, *Chem. Rev.*, **114**, 11503 (2014).
14. J. Xia, M. Nie, J. C. Burns, A. Xiao, W. M. Lamanna, and J. R. Dahn, *J. Power Sources*, **307**, 340 (2016).
15. A. J. Gmitter, I. Plitz, and G. G. Amatucci, *J. Electrochem. Soc.*, **159**, A370 (2012).
16. R. Petibon, J. Xia, L. Ma, M. Bauer, K. Nelson, and J. R. Dahn, *J. Electrochem. Soc.*, **163**, A2571 (2016).
17. J. Xia, R. Petibon, D. Xiong, L. Ma, and J. R. Dahn, *J. Power Sources*, **328**, 124 (2016).
18. R. Petibon, L. Rotermund, K. J. Nelson, A. S. Gozdz, J. Xia, and J. R. Dahn, *J. Electrochem. Soc.*, **161**, A1167 (2014).
19. D. Chalasani, J. Li, N. M. Jackson, M. Payne, and B. L. Lucht, *J. Power Sources*, **208**, 67 (2012).
20. N. N. Sinha, A. J. Smith, J. C. Burns, G. Jain, K. W. Eberman, E. Scott, J. P. Gardner, and J. R. Dahn, *J. Electrochem. Soc.*, **158**, A1194 (2011).
21. L. J. Krause, L. D. Jensen, and J. R. Dahn, *J. Electrochem. Soc.*, **159**, A937 (2012).

Downloaded on 2018-04-23 to IP 73.168.61.127 address. Redistribution subject to ECS terms of use (see ecsdl.org/site/terms_use) unless CC License in place (see abstract).

22. A. J. Smith, J. C. Burns, D. Xiong, and J. R. Dahn, *J. Electrochem. Soc.*, **158**, A1136 (2011).
23. J.-Y. Eom, I.-H. Jung, and J.-H. Lee, *J. Power Sources*, **196**, 9810 (2011).
24. K. Kumai, H. Miyashiro, Y. Kobayashi, K. Takei, and R. Ishikawa, *J. Power Sources*, **81–82**, 715 (1999).
25. J.-M. Atebamba, J. Moskon, S. Pejovnik, and M. Gaberscek, *J. Electrochem. Soc.*, **157**, A1218 (2010).
26. J. C. Burns, X. Xia, and J. R. Dahn, *J. Electrochem. Soc.*, **160**, A383 (2012).
27. H. M. Dahn, A. J. Smith, J. C. Burns, D. A. Stevens, and J. R. Dahn, *J. Electrochem. Soc.*, **159**, A1405 (2012).
28. I. Bloom, A. N. Jansen, D. P. Abraham, J. Knuth, S. A. Jones, V. S. Battaglia, and G. L. Henriksen, *J. Power Sources*, **139**, 295 (2005).
29. K. Honkura, H. Honbo, Y. Koishikawa, and T. Horiba, *ECS Trans.*, **13**, 61 (2008).
30. S. L. Glazier, L. E. Downie, J. Xia, A. J. Louli, and J. R. Dahn, *J. Electrochem. Soc.*, **163**, A2131 (2016).
31. L. E. Downie, S. R. Hyatt, A. T. B. Wright, and J. R. Dahn, *J. Phys. Chem. C*, **118**, 29533 (2014).
32. L. E. Downie, S. R. Hyatt, and J. R. Dahn, *J. Electrochem. Soc.*, **163**, A35 (2016).
33. L. E. Downie and J. R. Dahn, *J. Electrochem. Soc.*, **161**, A1782 (2014).
34. J. Taylor, *Introduction to Error Analysis, the Study of Uncertainties in Physical Measurements*, 2nd Edition, (1997).
35. J. C. Burns, A. Kassam, N. N. Sinha, L. E. Downie, L. Solnickova, B. M. Way, and J. R. Dahn, *J. Electrochem. Soc.*, **160**, A1451 (2013).

Downloaded on 2018-04-23 to IP **73.168.61.127** address. Redistribution subject to ECS terms of use (see **ecsdl.org/site/terms_use**) unless CC License in place (see abstract).